TURBULENCE STRUCTURAL MEASUREMENTS USING A COMPREHENSIVE LASER-DOPPLER VELOCIMETER IN TWO- AND THREE-DIMENSIONAL TURBULENT BOUNDARY LAYERS

K. Todd Lowe
Applied University Research, Inc.
605 Preston Avenue
Blacksburg, Virginia, 24060 USA
Corresponding author: toddlowe@aurinc.com

Roger L. Simpson
Department of Aerospace and Ocean Engineering
Virginia Tech
215 Randolph Hall
Blacksburg, Virginia, 24061 USA

ABSTRACT

The advanced 'comprehensive' laser Doppler velocimeter is used to acquire spatially and temporally resolved turbulence structural measurements in high Reynolds number two- and three-dimensional turbulent boundary layers. The new instrument directly measures three-dimensional particle trajectories at high repetitions. These trajectories are analyzed in post-processing to obtain fluctuating velocity gradient tensor fields, which lead to direct measurements of turbulent viscous dissipation rates. Such data acquired in two- and three-dimensional boundary layers with approach flow momentum thickness Reynolds number, $\mathrm{Re}_\theta = 7500$ are presented. Results indicate that anisotropy of the dissipation rate of Reynolds stresses persists to similar heights in viscous wall units as obtained with direct numerical simulations at lower Reynolds numbers. Measurements in a three-dimensional turbulent boundary layer in the vicinity of a wing/body junction also indicate that a reduction in the value of the velocity/pressure-gradient correlations for the Reynolds normal stresses reduces the turbulent energy redistribution and contributes to reduced shear stress magnitudes, as observed previously through DNS (Moin et al. 1990).

INTRODUCTION

Understanding the turbulence transport in shear flows is a key topic in fundamental research due to the immediate implications that the Reynolds stress transport equations have on modeling for the Reynolds stresses. Although the most-obvious uses for the models of the turbulence structural (transport) terms is in Reynolds-averaged Navier-Stokes (RANS) solutions, other solution techniques benefit from the information obtained by studying Reynolds-averaged turbulence structure. For instance, hybrid LES/RANS approaches have been developed and shown to be much more computationally efficient than LES and produce promising results (Labourasse and Sagaut 2002).

The Reynolds stress transport equations are given as

$$\frac{D\overline{u_i u_j}}{Dt} = P_{ij} + \Pi_{ij} + \nu\nabla^2\overline{u_i u_j} - \varepsilon_{ij} - \frac{\partial\overline{u_i u_j u_k}}{\partial x_k} \qquad (1)$$

where the production rate of the Reynolds stress tensor, $\overline{u_i u_j}$, is $P_{ij} = -\overline{u_i u_k}\partial\overline{U_j}/\partial x_k - \overline{u_j u_k}\partial\overline{U_i}/\partial x_k$, the velocity-pressure-gradient tensor is $\Pi_{ij} = -(1/\rho)\overline{u_i(\partial p/\partial x_j) + u_j(\partial p/\partial x_i)}$ with p being the fluctuating static pressure, the dissipation-rate tensor is $\varepsilon_{ij} = 2\nu\overline{(\partial u_i/\partial x_k)(\partial u_j/\partial x_k)}$, and ν is the kinematic viscosity. Each of the terms with the exception of Π_{ij} in equation (1) may be measured using the 'comprehensive' laser-Doppler velocimeter (CompLDV) described by Lowe (2006) and Lowe and Simpson (2007). To obtain transport rate budgets, Π_{ij} is determined by the balance of equation (1) using direct measurements for each of the terms therein, including the non-isotropic dissipation rate tensor, ε_{ij}. The dissipation rate tensor is directly evaluated from velocity gradient measurements that are possible with the unique capabilities of the CompLDV to be discussed.

By determining the non-isotropic dissipation rate directly and without the use of Taylor's Hypothesis and anisotropy models, a higher fidelity measurement of the velocity-pressure gradient tensor, Π_{ij}, is possible in high Reynolds number flows that cannot be simulated by direct numerical simulations (DNS). The importance of the velocity-pressure gradient term in wall-bounded three-dimensional (3D) flows has been shown for low Reynolds numbers by the DNS of Coleman et al. (2000). In the strained channel flow DNS, those authors discovered that Π_{ij} is of primary importance to the evolution of the Reynolds stresses. They showed that the lag between the mean shear rate and the Reynolds shear stresses, a key modeling problem in 3D flows, is primarily due to this term. Understanding the role of the velocity-pressure-gradient tensor in redistributing the Reynolds stresses is a key to improved modeling for the future of RANS and hybrid LES/RANS approaches.

The direct measurement of velocity gradients for determining non-isotropic dissipation rates has received much attention in experimental fluid mechanics, due to the fundamental need for such measurements. Several researchers have utilized a number of techniques for making turbulent velocity gradient measurements, such as hot-wire anemometry (Wallace and Foss 1995), particle image velocimetry (Meneveau and Katz 2000; Mullin and Dahm 2006), and laser-Doppler velocimetry (LDV; Tarau et al. 2002; Yao et al. 2001; Agui and Andreopoulos 2002). The reader is referred to Lowe (2006) for a more extensive review of the prior art in velocity gradient measurements. All the prior methods examined for turbulent velocity gradient measurements suffer from significant limits in spatial resolution and/or velocity dynamic range and are of limited applicability to high Reynolds number flows. This void is partially filled by the new CompLDV technologies discussed herein.

THE COMPREHENSIVE LDV TECHNIQUE

The CompLDV technique is capable of making highly-resolved particle trajectory measurements in turbulent flows (Lowe 2006; Lowe and Simpson 2007). The technique is based upon the principles of Gaussian beam coherent laser interference and Doppler shift due to particle scattering so that the instrument is closely related to the LDV technique. The CompLDV employs a novel optical arrangement to achieve low-uncertainty, time-resolved measurements of three-components each of particle position, velocity, and acceleration. In this work, the use of such measurements for directly estimating velocity gradients is explored.

The key development for measuring velocity gradients with this technique is the capability to measure positions of successively arriving particles at very high spatial resolution. In past work, sub-measurement volume position resolution LDV techniques have been developed (Czarske 2001; Czarske et al. 2002). These methods employ interference fringe patterns with calibrated spatial variations to obtain particle position resolutions at two-orders of magnitude smaller than the measurement volume diameter. This same fundamental concept is used in the CompLDV described herein and by Lowe (2006) and Lowe and Simpson (2007). The reader is referred to the paper by Czarske et al. (2002) for further details about fundamentals of particle position sensing in LDV.

To exhibit the capabilities of the CompLDV for particle position measurement, velocity profile measurements in two-dimensional (2D) flat plate TBLs are presented in Figure 1. These data have been obtained in the Department of Aerospace and Ocean Engineering Boundary Layer Research Wind Tunnel at Virginia Tech. CompLDV measurements at two momentum thickness Reynolds numbers ($\mathrm{Re}_\theta \equiv U_\infty \theta / \nu$, where θ is the momentum thickness), $\mathrm{Re}_\theta = 5930$ and $\mathrm{Re}_\theta = 7500$ are plotted. To obtain these data, measurements were acquired at six individual positions of the center of the measurement volume relative to the wall. The data presented are the mean stream-wise velocity statistics that have been divided among bins according to the normal-to-wall particle positions measured relative to the measurement volume center. When normalized with viscous wall scaling using the skin friction velocity as the velocity scale, $U^+ \equiv U / u_\tau$, and the viscous length scale to normalize the vertical height, $y^+ \equiv y/\delta_\nu = y u_\tau / \nu$, the comparison with previous conventional LDV data of DeGraaff and Eaton (2000) at a comparable Reynolds number along with the DNS data of Spalart (1988) at a lower Reynolds number is excellent, particularly in the viscous sublayer.

VELOCITY GRADIENT MEASUREMENT CONCEPT

The problem of estimating velocity gradients from CompLDV data is posed as follows:

Given the velocities and relative positions of N particles ($N \geq 4$), determine the velocity gradient tensor that is consistent with the data within experimental uncertainties and the constraints imposed by coherent turbulence scales.

The geometry of the problem is shown schematically in Figure 2. The particles arrive randomly in space and time. The statistics of the arrivals depend on the turbulence level as well as the velocity gradients across the volume (Albrecht et al. 2003). In the case of zero turbulence and velocity gradient, the arrival time statistics follow a Poisson (exponential) distribution, while the particles are uniformly distributed in space. The probability distribution function (PDF) of the measurement-volume validation weights the arrival position so that the measured positions are not uniformly distributed. The extrapolated volume, as depicted in Figure 2 is aligned approximately with the mean flow direction in the case that turbulent flow angles are relatively small.

A technique for estimating the velocity gradients from data as in Figure 2 is developed based upon an over-constrained system for the *N*-particles that cross the measurement volume within the allowable time *t*. To construct a least-squares cost function, some model for the distribution of the measured quantities must be assumed. In this case, we desired a coherent-structure-based model for the velocity field observed over a short record of time. The model assumed is a swirling structure aligned with the nominal mean flow direction and with a relatively large extent in space for that direction. The near-wall coherent structures in the 2DFPTBL such as the quasi-stream-wise vortex of Robinson (1991) have been observed to be consistent with this model. Further from the wall, it is still observed that the stream-wise 'legs' of 'crescent-shaped' structures are those that contribute to dissipation of the turbulence energy in the Reynolds stresses as the legs stretch and the vorticity within is intensified. The existence of these elongated dissipative structures gives credence to a technique that utilizes a long-narrow region of fluid as the basis for obtaining resolved velocity gradients. A simple structure of the velocity distribution is assumed such that the nine Cartesian-components of the velocity gradient tensor are modeled as constant within the observed region of flow.

To implement the model chosen, we refer again to Figure 2. The centroid velocity and position of the *N* particles may be readily obtained from the measured Doppler data. In the case that the velocity field assumed is exact and the measurements are without uncertainty, then a velocity gradient field which is consistent with the measurements will result in the following relationship:

$$(U,V,W)_i = (U,V,W)_c + \left[(\vec{r}_i - \vec{r}_c) \cdot \vec{\nabla} \right] (U,V,W)_c \qquad (2)$$

where $\vec{r}_i$ is the position vector of the i^{th} particle, $\vec{U}_i = U_i \hat{i} + V_i \hat{j} + W_i \hat{k}$ is the velocity vector of the i^{th} particle, $\vec{r}_c$ is the position vector of the centroid of the *N* particles considered for velocity gradient tensor estimation, and

$\bar{U}_c = U_c\hat{i} + V_c\hat{j} + W_c\hat{k}$ is the centroid velocity vector for the N particles. Equations (2) may also be thought of as the 3D Taylor-series expansions for the velocity components truncated for velocity derivatives of order 2 and greater [although one may refine velocity estimates using the CompLDV acceleration measurements to enhance the order of the method (Lowe and Simpson 2006)]. In the CompLDV measurements, uncertainty exists both for the measurements obtained as well as for the model equations (2). To mitigate this, redundant measurements for several particles are used along with equations (2) to construct objective cost functions that must be minimized by successive guesses for the velocity-gradient tensor. The cost function chosen is a least-squares error function developed from equation (2):

$$\Phi_{U,V,W} = \sum_{i=1}^{N} \left\{ (U,V,W)_c + \left[(\vec{r}_i - \vec{r}_c) \cdot \vec{\nabla} \right] (U,V,W)_c - (U,V,W)_i \right\}^2 \quad (3)$$

where $\Phi_{U,V,W}$ represents the three cost functions that are minimized to obtain the velocity gradient estimates. Note that in this implementation, the velocity components are decoupled except in the convection velocities that are hidden in the calculation of the position vectors:

$$\vec{r}_i = U_i(t_0 - t_A)\hat{i} + [y_i + V_i(t_0 - t_A)]\hat{j} + [z_i + W_i(t_0 - t_A)]\hat{k} \quad (4)$$

where t_A is the arrival time for the i^{th} particle, t_0 is the time at which the centroid information is computed, and y_i and z_i are the position components directly measured by the CompLDV. It is taken that the arrival time measurement for the burst occurs when the particle is at the location $x_i=0$, which is an excellent assertion considering the overall length of the volume under consideration.

The least-squares technique was tested using a Monte Carlo simulation to ensure that the optimization scheme would return the proper velocity gradient tensor with no uncertainties input. Details of this simulation may be found in the description by Lowe (2006). The resulting statistics indicated that the mean velocity gradient input was recovered with less than 5% discrepancy, while the artificial turbulence levels, indicative of fluctuating gradient uncertainties, were on the order of $\delta\overline{(\partial u_i / \partial x_j)^2}^{+} < 4E-4$ at 95% confidence (where the superscript + indicates viscous scaling). For comparison, typical values in the 2DFPTBL at $y^+=100$ for the mean-square fluctuation tensor are $\overline{(\partial u_i / \partial x_j)^2}^{+} \approx 0.003-0.006$ with the exception of the stream-wise velocity gradient along the same direction which is smaller, *O(0.001)*. Since the x-position is measured at such a small relative uncertainty (see Figure 2), the artificial stream-wise velocity gradients fluctuations were observed from the simulation to be $\delta\overline{(\partial u_i / \partial x)^2}^{+} < 4E-7$ at 95% confidence, indicating that the complete tensor could be measured at acceptable uncertainty levels.

RESULTS AND DISCUSSION

The technique for obtaining dissipation rate measurements was applied to the 2DFPTBL at $\mathrm{Re}_\theta = 7500$ and a 3D TBL alongside of a wing/body junction undergoing the same approach flow as the flat plate case.

In the case of the 2DFPTBL, the skin friction velocity was determined using a fit to the sublayer data shown in Figure 1 to obtain a result of $u_\tau = 1.02m/s$ for the approach velocity of $U_\infty = 28.0m/s$.

To implement the velocity gradient measurement scheme discussed above, time windows for accepting series of particles were determined based upon coherent structure convection velocities and sizes. For the coherent structures in the near-wall region, it has been observed that the convective speed of eddies is $U_C / u_\tau \approx 14$ (Ahn and Simpson 1987) and typical active near-wall structures exist in very long dimensions of x^+=500 or greater (Robinson 1991). From this, time windows were used that were always less than the ratio of the stream-wise length scale to the convective velocity scale. Additional details about the application of the technique are described by Lowe (2006).

The distributions of the Reynolds normal stress dissipation rates measured with the velocity gradient technique are plotted in Figure 3, normalized using wall variables. To the authors' knowledge, these measurements are the first of their kind at Reynolds numbers of this magnitude in turbulent boundary layers. The measurements in the $\mathrm{Re}_\theta = 7500$ flow closely follow the trends of the DNS data of Spalart (1988) at $\mathrm{Re}_\theta = 1410$. Note that anisotropy exists in the dissipation rate to values of y^+ of about 100, similar to the results obtained by Ölçmen and Simpson (1996) using the anisotropy model of Hallbäck et al. (1990) for the same flow. These results contradict simple blending function models such as the one due to Lai and So (2000), which gives isotropic predictions for y^+>10.

Using the dissipation rate data from Figure 3 and the velocity statistics data from the measurements, equation (1) may be used to extract the Π_{ij} profile. This term is plotted in Figure 4 for the $\mathrm{Re}_\theta = 7500$ 2DFPTBL in comparison with the DNS results of Spalart (1988) for $\mathrm{Re}_\theta = 1410$. While it is very difficult to validate such measurements due to the lack of information that exists for Π_{ij} at high Reynolds numbers, the similarity of the data to the wall-normalized DNS data gives confidence in the technique. Note that no profile smoothing has been used to obtain the results plotted.

Of even greater interest than the 2D case, the 3D attached turbulent boundary layer in the vicinity of a wing/body junction has been measured using the CompLDV. The geometry of the wing is a 3:2 elliptical nose joined at the maximum thickness to a NACA 0020 airfoil with a maximum thickness of 7.17cm. This particular flow was well-studied at Virginia Tech (Devenport and Simpson 1990; Ölçmen and Simpson 1995; Simpson 2001). The complex flow includes a chaotic separated region very near the junction of the wing, a highly-unsteady horseshoe vortex that is formed at the leading edge of the wing/body junction, and span-wise pressure gradients that generate stream-wise vorticity and strong three-dimensionality even outside of the attached vortex region at station 5.

The present CompLDV data were acquired at station 5, a location reported in previous work, located at (*x/t=0.026,z/t=-2.94*), where *x* is in the stream-wise direction and z is in the span-wise direction, both measured from the leading edge of the wing, and t is the maximum thickness of the wing. At this station, detailed, low-uncertainty conventional 3-component LDV data exist (Ölçmen and Simpson 1995, 1996). For consistency, the current data are compared with those of Ölçmen and Simpson in Figures 5-7. Note that the data in Figures 5 and 7 were reduced as volume-averaged statistics such that the effective measurement volume diameter for them was about $100 \mu m$. The mean velocities in this particular boundary layer profile are given in Figures 5 and 6 with comparisons between present data and those of Ölçmen and Simpson in both cases. The presentation of data in Figure 6 is directly analogous to those measurements in the 2DFPTBL in Figure 1, where several y-positions of data are obtained for single measurement volume positions by separating measurements into bins according to particle y-position data. Clearly, the multi-velocity-component operation of the CompLDV is seen therein, and these data were used to determine the skin friction velocity via a fit to the coplanar velocity gradient (Tang 2004) to be $u_\tau = 1.20 m/s$, which compares favorably within uncertainties with the value determined by Ölçmen and Simpson of $u_\tau = 1.15 m/s$. In Figure 7, the Reynolds normal stresses corrected for velocity gradient broadening (Durst et al. 1995) are compared with the results of Ölçmen and Simpson and indicate that the flow conditions were faithfully repeated in the currently reported experiment.

The dissipation rate measurement technique has been applied to the data for the wing/body junction flow. The transport rate budgets were computed using these non-isotropic dissipation rates and are presented in Figure 8. For these data, the boundary layer form of the Reynolds stress transport equations was considered such that only vertical gradients of Reynolds-averaged terms were computed. To obtain Π_{ij}, the balance of equation (1) was obtained using the non-isotropic dissipation rates. As noted by many previous authors, there is a reduction in the nearwall turbulent kinetic energy (TKE) and Reynolds shear stress for a wide array of 3D TBLs and correspondingly in the TKE and shear stress production, the present flow included (Simpson 2005; Coleman et al. 2000; Moin et al. 1990; Ölçmen and Simpson 1996). In the present data, reduction of the near-wall TKE and Reynolds shear stress production (not plotted) is accompanied by reduced values of Π_{ii} compared with the 2DFPTBL (Figure 9). This same result has been observed by Moin et al. (1990) through DNS. Those authors postulated that the reduction of shear stresses in their pressure-driven 3D flow was due to mechanisms that suppressed the redistribution of turbulent energy through Π_{ii}. The present results indicate that the stream-wise term Π_{11} is decreased from the 2DFPTBL case, though not as significantly as the production rate (Ölçmen and Simpson 1996). With reduced near-wall redistriubtion from the stream-wise normal stress and nearly zero redistribution of the span-wise normal stress that is being produced, the near-wall vertical normal stress receives less energy from those co-planar components. As noted by Moin et al. (1990), this mechanism of reduction of $\overline{v^2}$ in turn reduces production of shear stresses. The current data indicate a recovery of Π_{22} and Π_{33} to 2DFPTBL values above y^+=300, where $\overline{uv}$ shear stress levels reach approximately the same values as the 2DFPTBL (Ölçmen, M.S., and Simpson, R.L., 1996).

CONCLUSIONS

A novel experimental technique is reported for obtaining velocity gradients using highly resolved particle trajectory data in turbulent boundary layer flows. Results for non-isotropic dissipation rates in 2D and 3D turbulent boundary layers have been obtained. For the 2DFPTBL at $\mathrm{Re}_\theta = 7500$, the dissipation rate is anisotropic to approximatly the same viscous wall heights as in DNS for $\mathrm{Re}_\theta = 1410$. Measurements of the velocity/pressure-gradient correlation have been obtained in a 3D TBL in the vicinity of a wing/body junction. As in the 2DFPTBL, much of the transport profiles for the span-wise and vertical normal stresses are dominated by the dissipation rate and velocity/pressure gradient correlations. The results indicate a magnitude reduction in the velocity/pressure-gradient correlation in the near-wall region for each of the Reynolds normal stresses. These results corroborate the DNS results of Moin et al. (1990), that reduced energy redistribution contributes to reduced shear stress magnitudes frequently observed in an variety of 3D TBLs.

ACKNOWLEDGMENTS

This work was accomplished at the Virginia Tech Department of Aerospace and Ocean Engineering. The authors are grateful for the support provided by the National Science Foundation through grant CTS-0233653 under program manager Dr. Michael Plesniak and the Air Force Office of Scientific Research grant F49620-03-1-0057 under program manager Dr. Thomas Beutner.

REFERENCES

Agui, J.H. and Andreopoulos, Y., 2002 "A new laser vorticity probe--LAVOR: Its development and validation in turbulent boundary layer," ***Exp. in Fluids***, Vol. 34, No. 2, pp. 192-205.

Ahn, S. and Simpson, R.L. 1987, "Convective wave speed and spectral features of turbulent boundary layers" ***AIAA 25th Aerospace Sciences Meeting***, Paper AIAA-87-0198, Jan.12-15, Reno, NV.

Albrecht, H.-E., Borys, M. Damaschke, N., and Tropea, C. 2003 ***Laser Doppler and Phase Doppler Measurement Techniques*** Springer-Verlag, New York.

Czarske, J. 2001, "Laser-Doppler velocity profile sensor using a chromatic coding" ***Meas. Sci. Techn. 12,*** pp. 52-57.

Czarske, J., Büttner, L., and Razik, T. 2002, "Boundary layer velocity measurements by a laser-Doppler profile sensor with micrometre spatial resolution" ***Meas. Sci. Techn. 13***, 1979-1989.

DeGraaff, D.B. and Eaton, J.K. 2000 "Reynolds-number scaling of the flat-plate turbulent boundary layer," ***J. Fluid Mech.***, Vol. 422, pp. 319-346.

Devenport, W.J. and Simpson, R.L. 1990 "Time-dependent and time-averaged turbulence structure near the nose of a wing-body junction," ***J. Fluid Mech.***, **210**, p.23-55.

Durst, F., Jovanovic´, J., and Sender, J. 1995 "LDA measurements in the near wall region of a turbulent pipe flow," ***J. Fluid Mech.*** **295**, 305.

Hallbäck, M, Groth, J., and Johansson, A.V., 1990, "An algebraic model for non-isotropic turbulent dissipation rate in Reynolds stress closure, " ***Phys. Fluids***, Vol. 2, No. 10, pp. 1859-66.

Labourasse, E. and Sagaut, P. 2002 "Reconstruction of turbulent fluctuations using a hybrid RANS/LES approach," ***J. Comp. Physics,*** Vol. 182, No. 1, pp. 301-336.

Lai, Y.G. and So, R.M.C. 1990 "On near-wall turbulent flow modelling," ***J. Fluid Mech.*** Vol. 221, pp. 641-673.

Lowe, K.T., 2006 "Design and application of a novel Laser-Doppler Velocimeter for turbulence structural measurements in turbulent boundary layers," ***Ph.D. Dissertation,*** September, Department of Aerospace and Ocean Engr., Virginia Tech.

Lowe, K.T. and Simpson, R.L. 2006 "Measurements of velocity-acceleration statistics in turbulent boundary layers," ***Int. J. Heat and Fluid Flow,*** Vol. 27, No. 4, pp. 558-565

Lowe, K.T. and Simpson, R.L. 2007 "An advanced laser-Doppler velocimeter for three-component particle trajectory measurements, " ***in prep. for Meas. Sci. Technol.***

Meneveau, C. and Katz, J. 2000 "Scale-invariance and turbulence models for large-eddy simulation," ***Annu. Rev. Fluid Mech.***, Vol. 32, pp. 1-32.

Moin, P., Shih, T.-H., Driver, D., and Mansour, N.N. 1990 "Direct numerical simulation of a three-dimensional turbulent boundary layer, " ***Phys. Fluids A***, Vol. 2, No. 10, pp. 1846-53.

Mullin, J.A. and Dahm, W.J.A. 2006 "Dual-plane stereo particle image velocimetry measurements of velocity gradient tensor fields in turbulent shear flow. I. Accuracy assessments" ***Phys. Fluids, 18***, pp. 035101-1 to 035101-18.

Ölçmen, M.S., and Simpson, R.L., 1995, "An experimental study of a three-dimensional pressure-driven turbulent boundary layer," ***J. Fluid Mech.,*** Vol 290, 225-262.

Ölçmen, M.S., and Simpson, R.L., 1996, "Experimental transport-rate budgets in complex 3-D turbulent flow near a wing-body junction, " ***27th AIAA Fluid Mech. Conf.***, 17-20 June, New Orleans, LA, USA, paper 96-2035

Robinson, S.K. 1991 "Coherent motions in the turbulent boundary layer," ***Ann. Rev. Fluid Mech.***, Vol. 23, pp. 601-639.

Simpson, R.L. 2001 "Junction flows, " ***Ann. Rev. Fluid Mech***, Vol. 33, pp. 415-443.

Simpson, R.L. 2005 "Some observations on the structure and modeling of 3-D turbulent boundary layers," ***TSFP-5***, Vol. 1, 27-29 June, Williamsburg, VA, USA, pp. 1-10.

Spalart, P. 1988, "Direct simulation of a turbulent boundary layer up to $\mathrm{Re}_\theta = 1410$," ***J. Fluid Mech.,*** Vol. 187, pp. 61-98.

Tang, G. 2004 "Measurements of the Tip-gap Turbulent Flow Structure in a Low-speed Compressor Cascade," ***Ph.D. Dissertation***, April, Department of Aerospace and Ocean Engr., Virginia Tech.

Tarau, T., Stepaniuk, V.P., and Otugen, M.V., 2002 "Evaluation of a new laser gradient probe," ***40th Annual AIAA Aerospace Sciences Meeting and Exhibit,*** Jan. 14-17, Reno, NV, AIAA 2002-0688.

Wallace, J.M. and Foss, J.F. 1995 "The measurement of vorticity in turbulent flows," ***Annu. Rev. Fluid Mech.*** Vol. 27, pp. 469-514.

Yao, S., Tong, P., and Ackerson, B. J., 2001 "Proposal and testing for a fiber-optic-based measurement of flow vorticity: ***Applied Optics***, Vol. 40,No. 24, pp. 4022-4027.

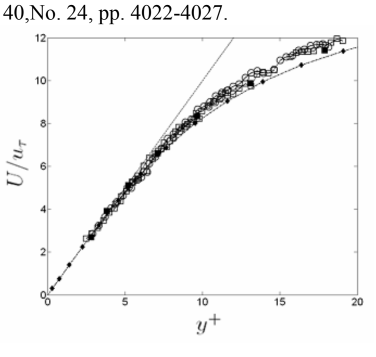

Figure 1.Resolved profiles for the mean stream-wise velocity in viscous wall scaling. □, Current data for $\mathrm{Re}_\theta = 5930$; ○, Current data for $\mathrm{Re}_\theta = 7500$; ■, LDV data of DeGraaff and Eaton (2000) for $\mathrm{Re}_\theta = 5160$. ◆, DNS data of Spalart (1988) for $\mathrm{Re}_\theta = 1410$. The dashed line in this plot is the viscous sublayer relationship, $U^+ = y^+$.

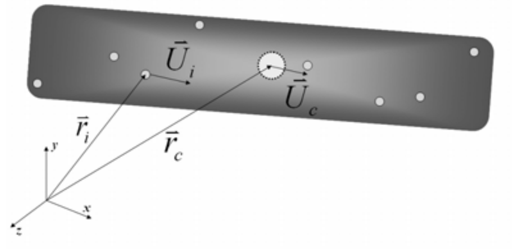

Figure 2. Schematic of an instance for the CompLDV extrapolated measurement volume containing several particles with measured velocities and positions. Symbols defined in text.

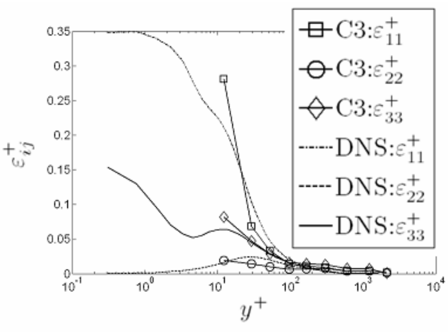

Figure 3. Non-isotropic Reynolds stress dissipation rate in the 2DFPTBL. C3, CompLDV data for $\mathrm{Re}_\theta = 7500$; DNS, simulation data of Spalart (1988) for $\mathrm{Re}_\theta = 1410$.

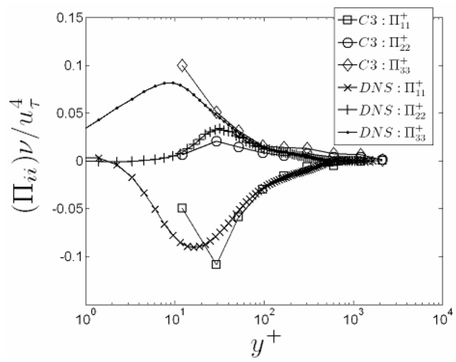

Figure 4. Velocity/pressure gradient correlation in the 2DFPTBL at $\mathrm{Re}_\theta = 7500$. C3, CompLDV; DNS, Simulation data of Spalart (1988).

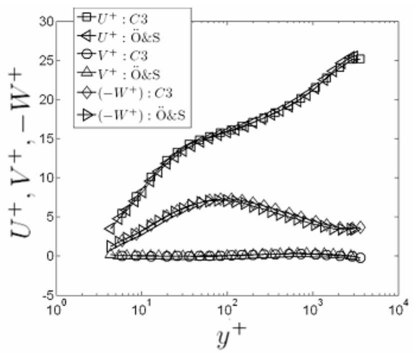

Figure 5. Mean velocities for the wing/body junction flow at station 5. C3: CompLDV; Ö&S: Ölçmen and Simpson (1995). 'Tunnel' coordinate system *x*axis is aligned with the inflow velocity vector and *y*-axis is normal-to-wall.

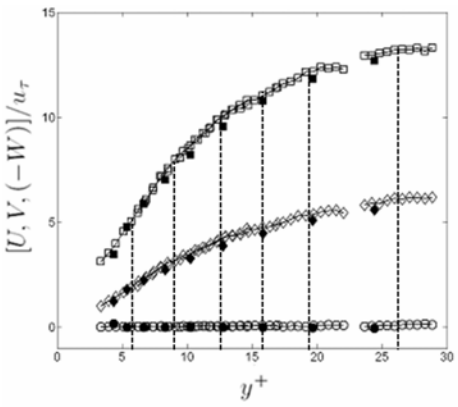

Figure 6. Sub-measurement volume resolution mean velocities for the wing/body junction flow at station 5. Symbols: □, $\overline{U}/u_\tau$; ○, $\overline{V}/u_\tau$; ◊, $-\overline{W}/u_\tau$. Open symbols are current CompLDV measurements; solid symbols are data of Ölçmen and Simpson (1995). Vertical dashed lines show center locations of measurement volume. Tunnel coordinate system.

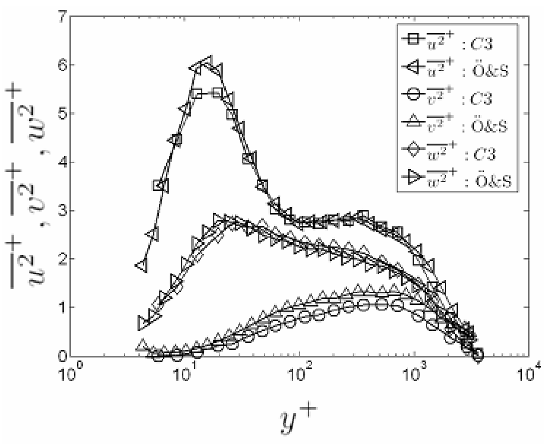

Figure 7. Reynolds normal stresses for the wing/body junction flow at station 5. C3: CompLDV; Ö&S: Ölçmen and Simpson (1995). Tunnel coordinate system.

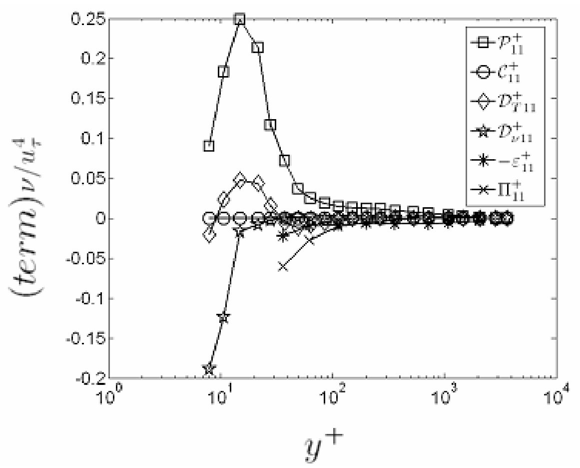

Figure 8 (a)

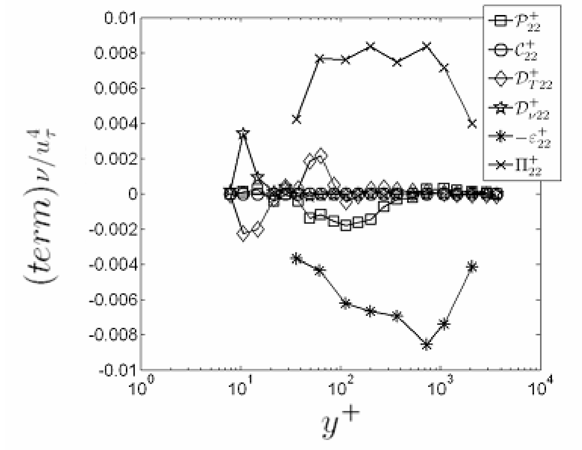

Figure 8 (b)

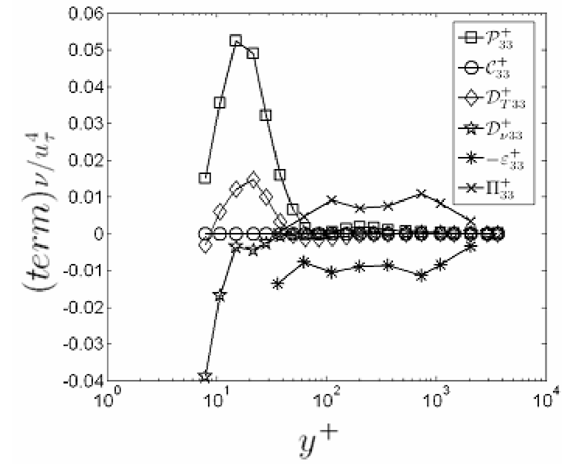

Figure 8 (c)

Figure 8. Reynolds stress transport balances using the non-isotropic dissipation rates for the wing/body junction flow at station 5.

(a) $\overline{u^2}^+$, (b) $\overline{v^2}^+$, (c) $\overline{w^2}^+$,

$\mathcal{P}_{ij}$=Production; $\mathcal{C}_{ij}$=Convection; $\mathcal{D}_{\nu ij}$=Viscous diffusion; $\mathcal{D}_{Tij}$=Turbulent diffusion; ε_{ij}=Dissipation rate; Π_{ij}=Velocity/pressure gradient correlation. Tunnel coordinate system.

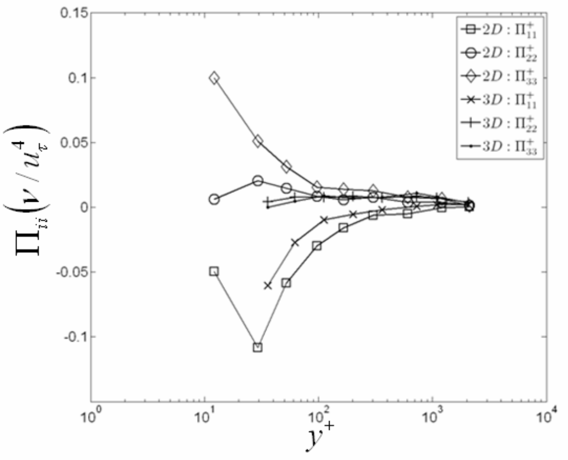

Figure 9. Comparison of 2DFPTBL (2D) and 3D TBL(3D) results for Π_{ij}.